JTTEE5 18:272–283
DOI: 10.1007/s11666-009-9295-4
1059-9630/$19.00 © ASM International

Manufacturing Process of Nanostructured Alumina Coatings by Suspension Plasma Spraying

Changjun Qiu and Yong Chen

(Submitted April 16, 2008; in revised form July 3, 2008)

This paper describes the formation process of nanostructured alumina coatings and the injection system obtained by suspension plasma spraying (SPS), an alternative to the atmospheric plasma spraying technique in which the material feedstock is a suspension of the nanopowder to be sprayed. The nanoscale alumina powders ($d \approx 20$ nm) were dispersed in distilled water or ethanol and injected by a peristaltic pump into plasma under atmospheric conditions. Optical microscopy (OM), scanning electron microscopy (SEM), and x-ray diffraction (XRD) analyses were performed to study the microstructure of the nanostructured alumina coatings. The results showed that the nanoscale alumina powders in suspension were very easily adsorbed at the inner surface of injection, which caused the needle to jam. The rotation of the pump had a great effect on the suspension injection in the plasma. The very small resistance of the thin plasma boundary layer near the substrate can drastically decrease the impacting velocity of nanosize droplets. The concentration of suspension also has a significant influence on the distribution of the size of the droplet, the enthalpy needed for spraying suspension, and the roughness of the coating surface. The phase structures of alumina suspension coatings strongly depend on the plasma spraying distance. A significant nanostructured fine alumina coating was obtained in some areas when ethanol was used as a solvent. The microstructures of the coating were observed as a function of the solvent and the spraying parameters.

Keywords nanoscale alumina powders, nanostructured alumina coatings, suspension plasma spraying

1. Introduction

Alumina ceramics are widely used as wear-resistant and insulating coatings. Atmospheric plasma spraying (APS) is a common method for preparing Al_2O_3 coatings (Ref 1). A new interest in nanostructured coatings, with grain sizes smaller than 100 nm, has recently emerged. This is due to the enhanced properties of the nanoscale effect. Depending on the processing conditions, they can exhibit superior performance when compared with conventional coatings. The processing of nanostructured coatings has also reached the field of thermal spray, in which they have also shown superior performance when compared with conventional coatings (Ref 2-6).

Many articles and much information about nanostructured coatings formed by chemical vapor deposition (CVD) and plasma vapor deposition (PVD) can be found. When their crystallite size is less than 100 nm, the nanocrystallite coatings demonstrate superior mechanical performance when compared with conventional coatings (Ref 7, 8). Several attempts have been made to deposit nanostructured coatings by thermal spraying. These attempts can be divided into five categories (Ref 4). In the first type, which is the most widely used, micron-sized powders are deformed heavily by mechanical alloying to get the nanoscale structure and then sprayed. In the second approach, nanosize powders are sprayed directly. The third type of effort consists of spraying the nanopowder with gaseous precursors. The fourth variety is spraying the powders with liquid precursors. The fifth method of spraying nanostructured coatings involves designing alloys with a low critical cooling rate so that upon spraying they become amorphous. They are then heated above their crystallization temperature to initiate diversification (Ref 4, 9-15).

In recent years, some commercially available nanostructured powders, which consisted of agglomerated particles of 15 to 150 μm in diameter with nanoscale grains, were used to deposit nanostructured coatings by atmospheric plasma spraying without changing the APS system. That kind of nanostructured coating exhibits better mechanical properties than conventional coatings of the same composition (Ref 16-18). The nanostructured fine coating fabricated by the suspension plasma spraying process, in which the nanosize powders were dispersed in distilled solvent and injected by peristaltic pump in plasma under atmospheric conditions directly, mainly focused on the solid oxide fuel cell (SOFC) electrolytes as well as photocatalytic titania coatings (Ref 19, 20). The aim of this work was to use the functional properties of

Changjun Qiu and **Yong Chen**, College of Mechanical Engineering, University of South China, Hengyang 421001, China. Contact e-mail: qiuchangjun@hotmail.com.

nanostructured coatings. The mechanical properties of nanostructured WC-Co coatings formed by the suspension plasma spraying process were investigated. The results showed that the coating hardness is a strong function of porosity and the degree of carbide degradation is lower than that of conventional coatings (Ref 14, 21). Many routes of producing finely structured coatings by thermal spray techniques have been introduced (Ref 22). In the thermal spray literature, the feasibility study on the use of smaller nanoscale alumina particles (less than 20 nm, in diameter) to form the nanostructured coatings by the suspension plasma spraying process directly were ignored. In this study, the nanoparticles ($d \approx 20$ nm) were dispersed in distilled water or ethanol for suspension. This suspension was injected directly into the plasma. The fluid properties of the suspension in the injection system, the motion properties of the nanoscale droplet near the substrate, and the microstructure and phase of the coating were investigated.

2. Method

The experimental setup consists of a plasma torch, an injection system driven by a peristaltic pump for suspension, a pendulum to collect the droplets, and an optical window to view the plasma and injection. The injection system is composed of a peristaltic pump, the rotation of which can be easily adjusted, and a stainless steel injector with an inner diameter of 250 μm. The suspension is injected by controlling the rotation of the pump wheel. The pressure of injection was monitored with a pressure gage. The nanoparticles were very easily adsorbed in the inner surface of the injector, which can cause the pressure to increase. A quick increase in pressure indicates that the injector is closed by the nanoparticles adsorbed in the inner surface of the injector. The injector is fixed on a specially designed place, where the suspension penetrates the plasma at the counterflow. This nozzle is beneficial to improving the thermal treatment particles (Fig. 1).

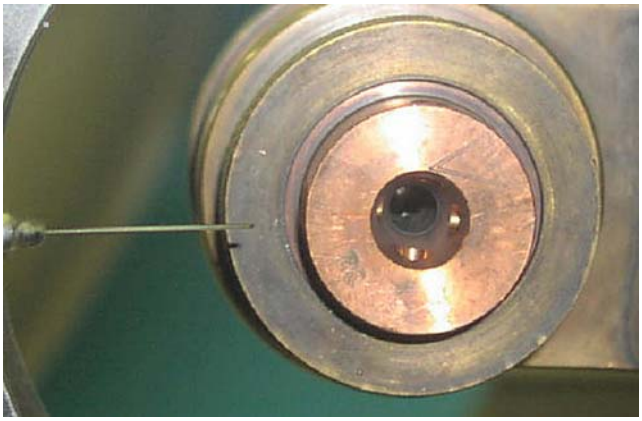

Fig. 1 System of injection

The efficient power of the plasma torch was between 18 and 51 kW with Ar/H_2 (40/6-12 slm) mixtures as plasma forming gases. The nozzle internal diameters were 6 mm. During all experiments, the condition of the plasma torch was measured and recorded by the computer. The mean diameter of the nanoscale alumina particles used in the experiment was 20 nm. The solvent was water or ethanol. Suspensions with 10 and 40 wt.% nanopowders were chosen, and an ultrasonic bath in 50 kHz was used to prevent the nanoparticles from agglomerating in the suspension. All substrates used for the experiments were under the normal temperature. The Hitachi S-4800 type scanning electron microscope (Hitachi company, Tokyo, Japan) was used to observe the microstructure of coatings and the powders; the Siemens D5000 x-ray diffractometer (Siemens company, Karlsruhe, Germany) was used to analyze the structure.

3. Results and Discussion

3.1 Properties of Injection System for Nanoparticle Suspension

Since the nanoparticles were very easily adsorbed at the inner surface of the injector, the flux of suspension at constant rotation of the pump was the function of time. This was very different from when the pure liquid was used. In the experiment, the inner diameter of the needle was 0.2 mm, the inner diameter of the tube was 3.2 mm, and the rotation of the pump was 50 rpm. After working for 20 min, the injection system was not stable (Fig. 2). This result indicated that the system could not continue work. So after working about 10-15 min, the system was cleared with a pure solvent to prevent the needle from being closed by the nanoparticles that were adsorbed at the inner surface of needle.

3.2 Effect of Pump Rotation on Injection

The pump feeder system turned out to be very pressure sensitive, especially when using nozzles with a 0.5 mm diameter (Ref 23). When the rotation speed was increased, the pressure, the flux, and the velocity of the injection would also increase. The rotation of the pump

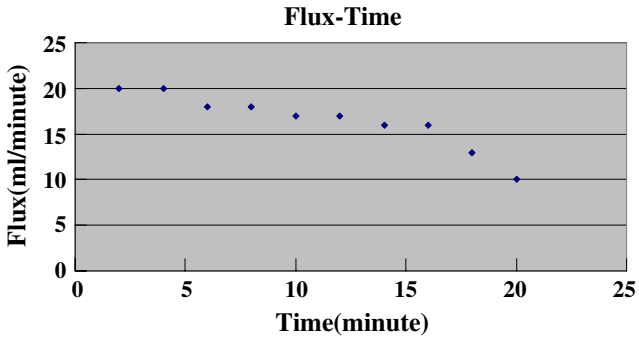

Fig. 2 Relation of flux varying with time

had a significant effect on the injection, the image of which was captured by a camera.

Figure 3(c) indicates that the rotation of the pump is so fast that it made the injection of water have enough momentum to change the direction of the plasma. In the experiment, the rotation of the pump was between 50 and 70 rpm.

3.3 Motion Properties of the Nanoscale Droplet Near the Substrate

Coating quality obtained during thermal spraying depends strongly on the dynamics of flattening the molten powder particles. The kinetics of the droplet flattening depended on the droplet size and impact

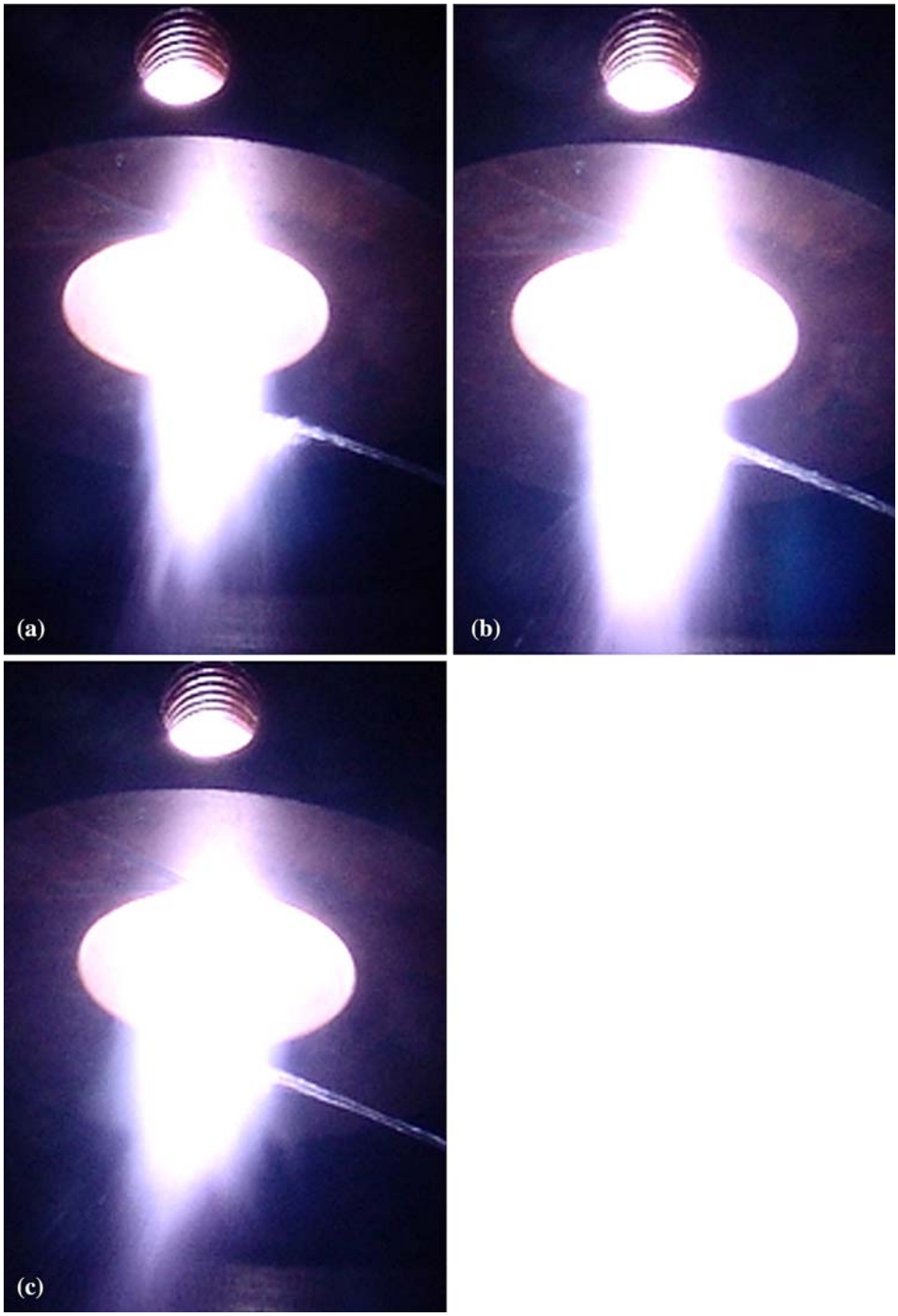

Fig. 3 The effect of the pump rotation on the plasma penetration. (a) 50 rpm. (b) 65 rpm. (c) 100 rpm

velocity (Ref 24). The very small particles were immediately accelerated to the plasma gas velocity (Ref 25). Spontaneously, these very small particles were immediately decelerated to zero as soon as they were near the substrate where the velocity of the plasma gas was zero. When the plasma velocity reached the supersonic level, a strong bow shock formed in front of the substrate that could cause the velocity of larger particles to decrease drastically (Ref 26). When the plasma velocity was below the sonic velocity, there was only a thin boundary layer, without bow shock, near the substrate. In conventional thermal spraying fields, since the droplets ($d > 5$ μm) have enough momentum to overcome the resistance of the thin plasma boundary layer near the substrate, the effect of the thin plasma boundary layer near the substrate on the impact of the droplet could be ignored. However, when the droplets became nanoscale, the smaller resistance near the substrate would have had a significant influence on the impact velocity of the nanoscale droplets. This is illustrated in Fig. 4.

As the critical situation, the droplet arrived at the surface of the substrate with the velocity 0 (zero).

We can get approximately (Ref 27):

$$u - V_p = -(x/H)^m(1 - x/H)V_0 \quad \text{(Eq 1)}$$

where x is the distance to the substrate and V_0 is the velocity of the plasma without the effect of the substrate;

$$(4/3)\pi \times (D_p/2)^3 \rho_p (dV_p/dt) = -C_D \times \pi \times (D_p/2)^2 (\rho_g/2)[(x/H)^m(1 - x/H)V_0]^2 \quad \text{(Eq 2)}$$

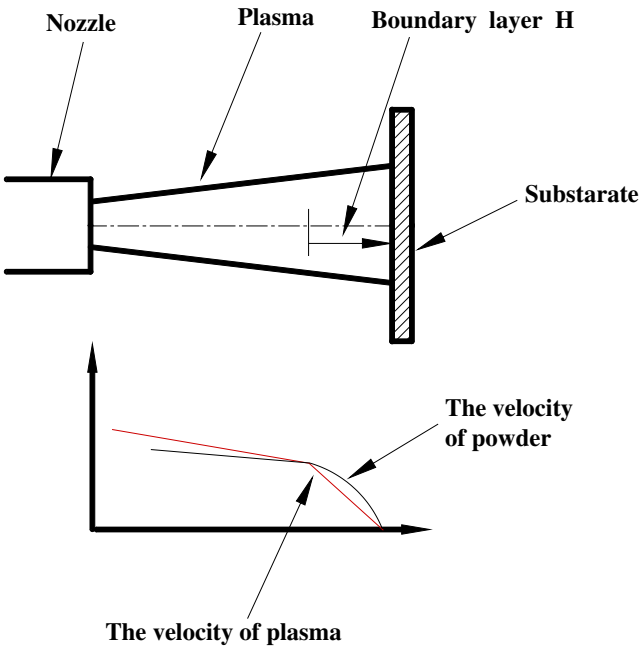

Fig. 4 Effect of the thin boundary layer on the velocity of the nanoscale droplet

Integrated from the 0 to H

$$V_p(4/3)\pi \times (D_p/2)^3 \rho_p dV_p = -C_D \times \pi \times (D_p/2)^2 (\rho_g/2)[(x/H)^m(1 - x/H)V_0]^2 dx \quad \text{(Eq 3)}$$

The critical diameter of the droplet could be found, which, with enough momentum, arrived at the surface of the substrate where velocity $u = 0$.

$$D_p = (3C_D \times H \times \rho_g)/[(2m + 1)(2m + 2)(2m + 3)\rho_p]$$

where $\rho_g = 0.08$ kg/m^3 (about 8000 °C, plasma), $C_D =$ (5-16) (Ref 28), $\rho_p = 3900$ kg/m^3, $H = 10$ mm, $m = 1.5$. The critical diameter of droplet is $D_p \approx 60$ nm.

D_p is the diameter of powder.
ρ_p is the density of powder.
ρ_g is the density of the plasma for spraying.
V_p is the velocity of the powder in the plasma.

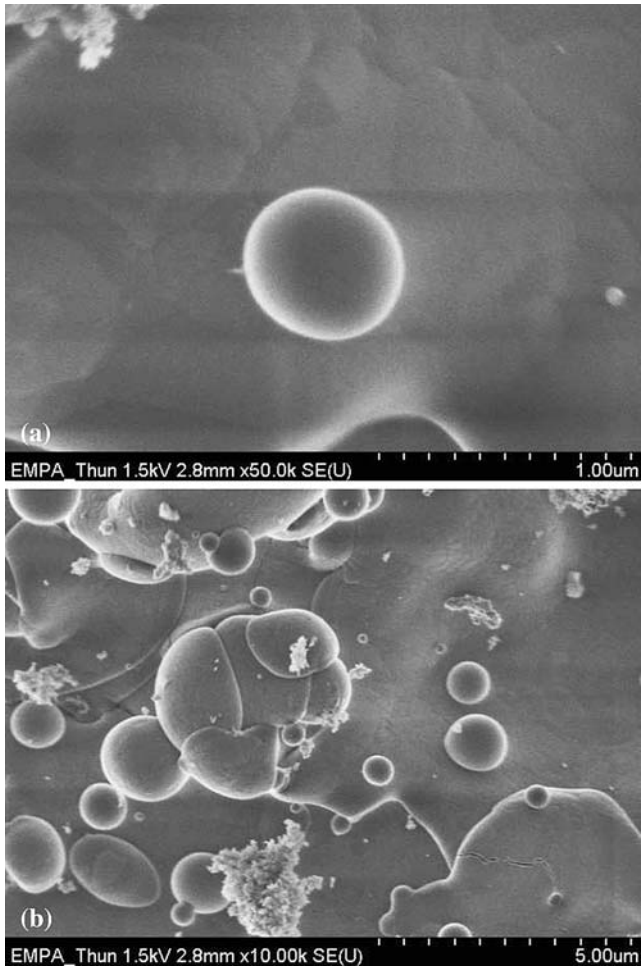

Fig. 5 Morphology of spherical alumina nanosize splats in alumina ethanol suspension plasma spray coatings. (a) A single splat morphology. (b) Different sizes of splats morphology

C_D is the coefficient of resistance (the powder moving in the plasma).

u is the velocity of the plasma.

H is the effective thickness of the substrate (within this distance the plasma velocity decrease from u to zero).

Based on the result, the droplets (with a diameter of less 60 nm and a density of 3900 kg/m^3) barely reach the substrate with enough velocity impacting the substrate to form a lamellar interface. This is because the momentum was too small to overcome the resistance of the plasma boundary layer near the substrate. The previous study showed that the flattening behavior of molten spray droplets on a surface is influenced by many factors. The impact velocity of droplets was one of the key factors. When only the impact velocity was changed, the splats showed a different morphology on the substrate. The morphology of splats was a function of the impact velocity of droplets (Ref 29, 30). Inversely, the impact velocity of droplets could be evaluated by the morphology of splats. The initial particle diameter could be calculated using the splat diameter (Ref 31). The droplets collected on the substrate that were generally larger than 300 nm in diameter showed impact deformation (Ref 2, 31). All alumina splats whose sizes were principally between 100 and 300 nm were spheroidized, and the alumina splats with a diameter of less than 100 nm

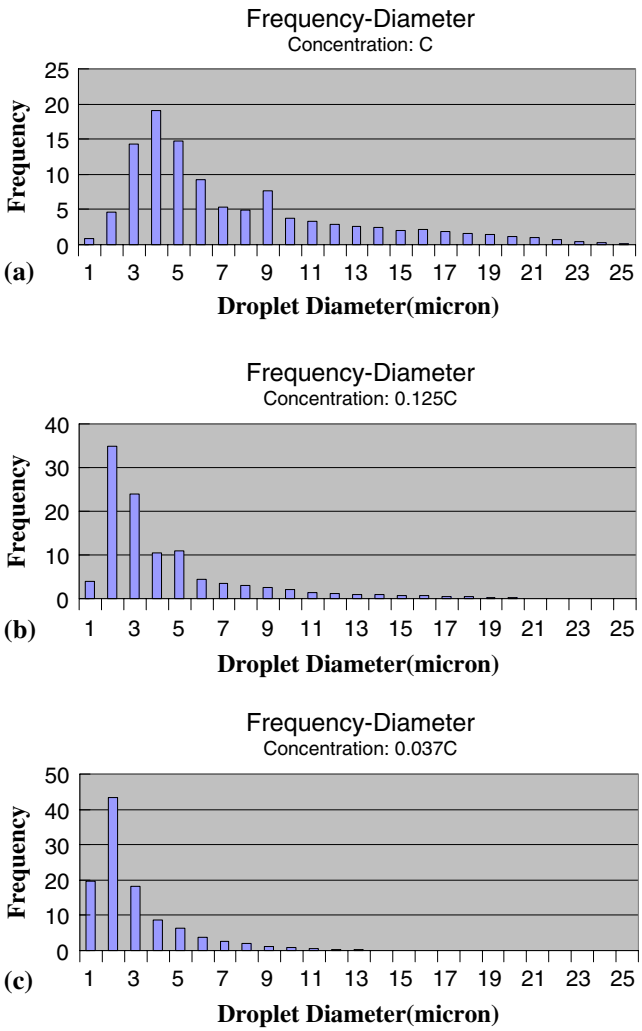

Fig. 6 The droplet diameter distribution. (a) Ref 34. (b) 0.125C. (c) 0.037C

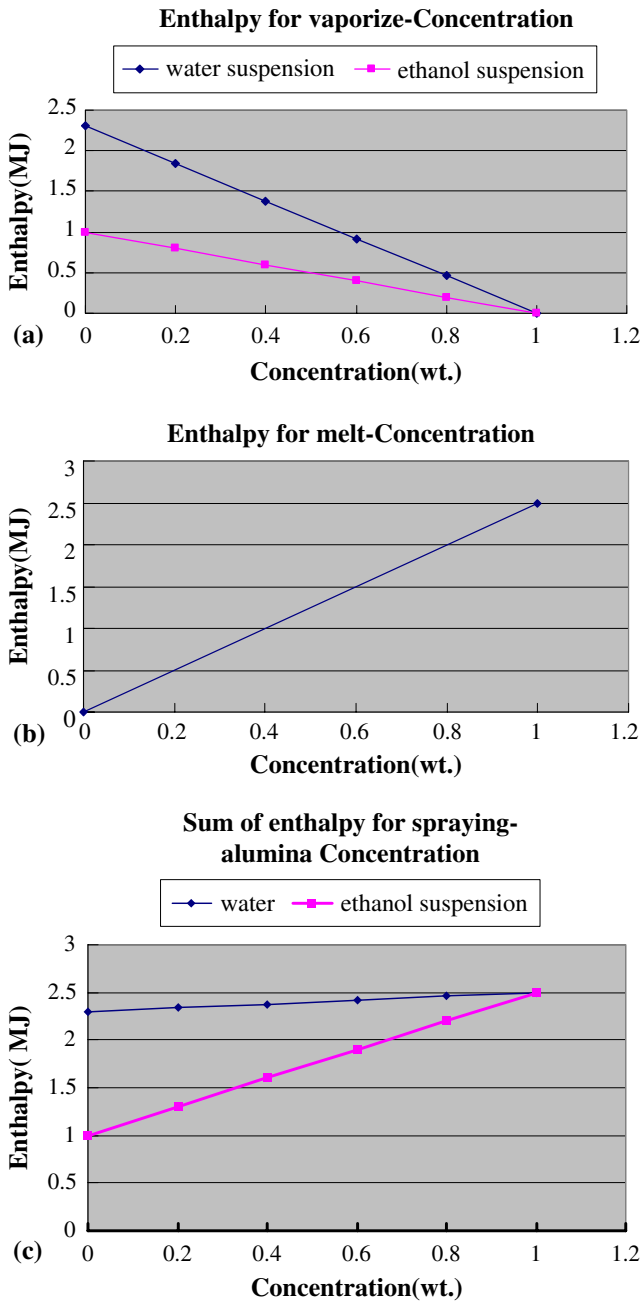

Fig. 7 The relation between enthalpy and concentration. (a) Only for vaporizing. (b) Only for heating and melting alumina. (c) Sum of enthalpy for vaporizing and melting

were barely observed on the substrate (Ref 2, 32, Fig. 5). This experimental result showed that the impact velocity of alumina droplets with size between 100 and 300 nm was very low. All of the experimental results were consistent with the theoretical analysis mentioned previously. Synchronously, since there was turbulence near the substrate, some small droplets with a diameter of less than 60 nm could reach the surface of the substrate at a low impact velocity. This would make the interface formed by these droplets very weak (Ref 33). This weak lamellar interface caused the macromechanical properties of the alumina suspension plasma spray coatings to degrade.

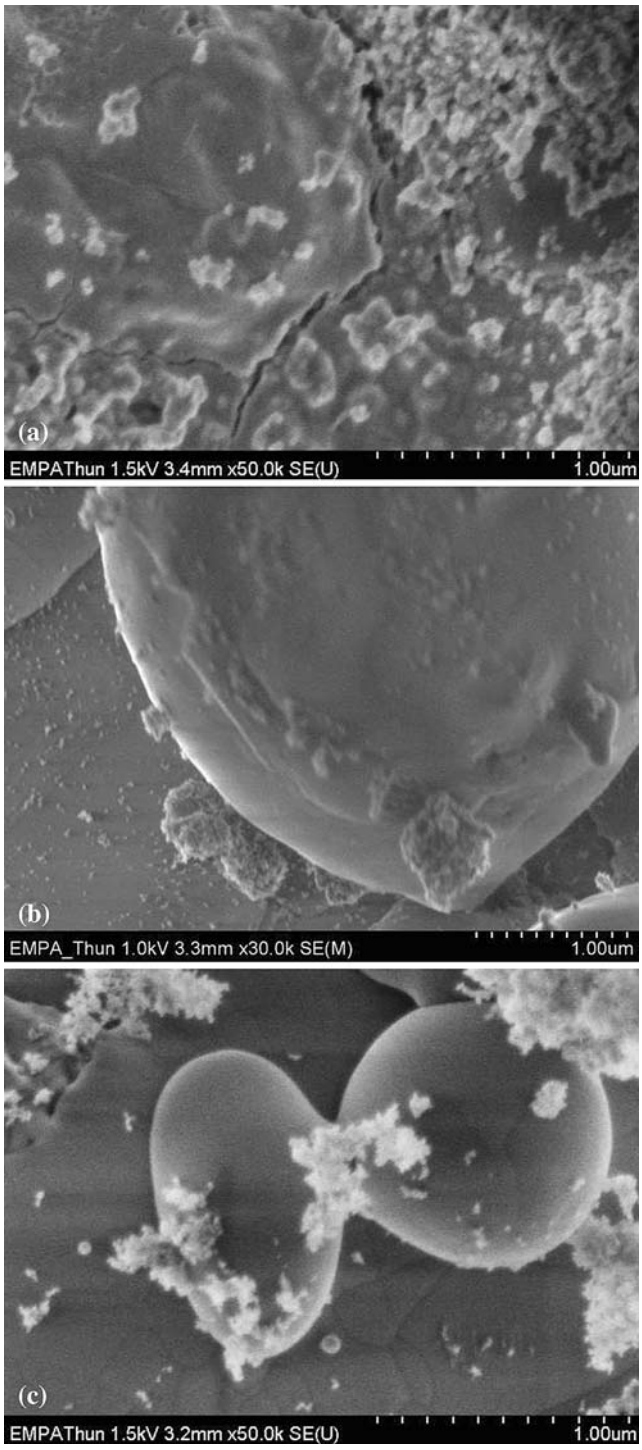

Fig. 8 Splat morphology at different concentration. (a) 40 wt.%. (b) 10 wt.%. (c) 5 wt.%. Operating conditions: 45 kW, 60 mm

3.4 Influence of Concentration

Based on the three-dimensional (3D) model and the numerical technique, the size distribution of the droplet on the substrate could be determined, just as Fig. 6(a) shows (Ref 34). If liquid fragmentation steps were supposed to be the same for different concentration suspensions, it was expected that a lower load led to a smaller size of the molten particle with a ratio of $(C_1/C_2)^{1/3}$ (Ref 31). According to the principle described in Ref 31, the distribution of the diameter of the droplet at different concentrations could be found (Fig. 6b, c).

The results demonstrate that, as the concentration was decreased, the size range of the droplet also decreased. This was beneficial for the fine nanostructure of coatings. On the other hand, a small concentration meant a low spraying efficiency.

According to the details in Ref 31: The Al_2O_3 melting point was 2345 K, the heat for melting was 1071.8 kJ/kg, and the specific heat was 800 J/kg K. The enthalpy needed to heat and melt 1 kg Al_2O_3 was 2.51 MJ. The enthalpy needed to heat and vaporize 1 kg ethanol was 1 MJ. The enthalpy needed to heat and vaporize 1 kg water was 2.3 MJ. From these details, the relations between the concentration and the enthalpy for spraying could be determined (Fig. 7).

Using the same operation: Plasma power was 45 kW, current was 700 A, Ar/H_2 was 40/8 slm. The different surface microstructures are shown in Fig. 8 at different suspension loads. No melting powder, bigger molten splats, and the crack caused by thermal concentration in big splats appeared on the surface of the high suspension load (40% wt., Fig. 8a). This result demonstrates that higher concentrations of suspension induce bigger droplets and need more energy for spraying.

The roughness of the alumina suspension plasma spray coating surface is shown in Table 1. The results demonstrated that low concentration induces a smooth coating surface. The original roughness of the substrate was 0.8 μm.

Table 1 Roughness of coating surface

Concentration, wt.%	Roughness (R_a), μm
40	3.3-4.8
10	1.8-2.9
5	1.2-2.2

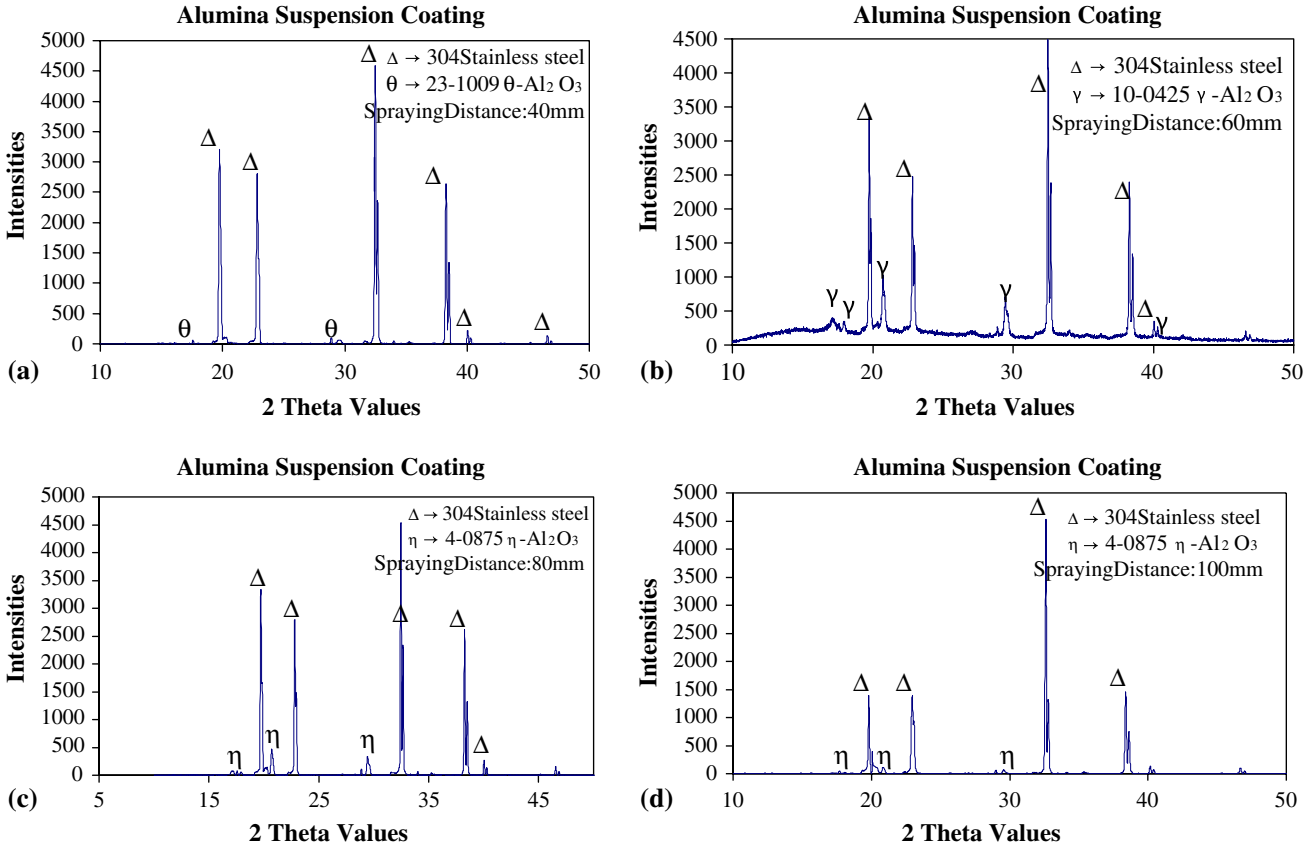

Fig. 9 XRD pattern of alumina ethanol suspension (10 wt.%) spray coatings at different spraying distances. (a) 40 mm. (b) 60 mm. (c) 80 mm. (d) 100 mm

3.5 Spraying Distance Effect on the Transformation of Alumina Phases

The phase selection in plasma sprayed alumina depended on the quenching conditions (Ref 35). The α-structured alumina can result from hexagonal packing of the oxygen atoms with aluminum atoms that have enough time to move into the available octahedral sites under equilibrium conditions. Under rapid quenching conditions, the tetrahedral coordinated aluminum atoms will primarily form transition aluminums, which are based on a modified cubic close-packed structure. Therefore, transition alumina will be formed first in preference to α-alumina after the melt droplet impacts the substrates. Furthermore, the temperature of the droplets, as well as the substrates, controls the quenching condition. The influence of the substrate temperature on the transformation of alumina phases had been researched. Since the droplet temperature strongly depends on the spraying distance at similar plasma operation conditions, (i.e., under the same substrate temperature the spraying distance controls the quenching ratio of splats, which were just impacting the substrate), the spraying distance is a key parameter for the transformation of the alumina phase. Figure 9 shows a gradual change of the phases of alumina depending on the plasma spraying distance.

The results demonstrate that the phase of alumina ethanol suspension plasma spray coatings is mainly a transition phase.

3.6 Microstructure of Powder and Coating

3.6.1 Microstructure of Powder. The suspension, without being processed by the plasma, was dried and observed with SEM. The results (Fig. 10) showed the diameter of the particles was about 20 nm in both different suspensions, but the nanoscale particles were agglomerated in the suspension. The x-ray diffraction patterns (XRD) of the dried powder are illustrated in Fig. 11.

3.6.2 Microstructure of Coatings at Different Spraying Conditions. The photographs show the surface of coatings in which water was used as a solvent (Fig. 12). The results showed the particles were not melted, and the nanoparticles appeared agglomerated (Fig. 12b). The conditions of the experiment are listed in Table 2.

Figure 13 shows the photographs of the alumina ethanol suspension plasma spray coatings surface. The result indicates that splats melted, the nanostructured surface was demonstrated, and the nanoscale was between 30 and 100 nm (Fig. 13b). The melted and unmelted areas were found on the surface of this sample (Fig. 14). In the unmelted area, all of the nanoparticles appeared in an

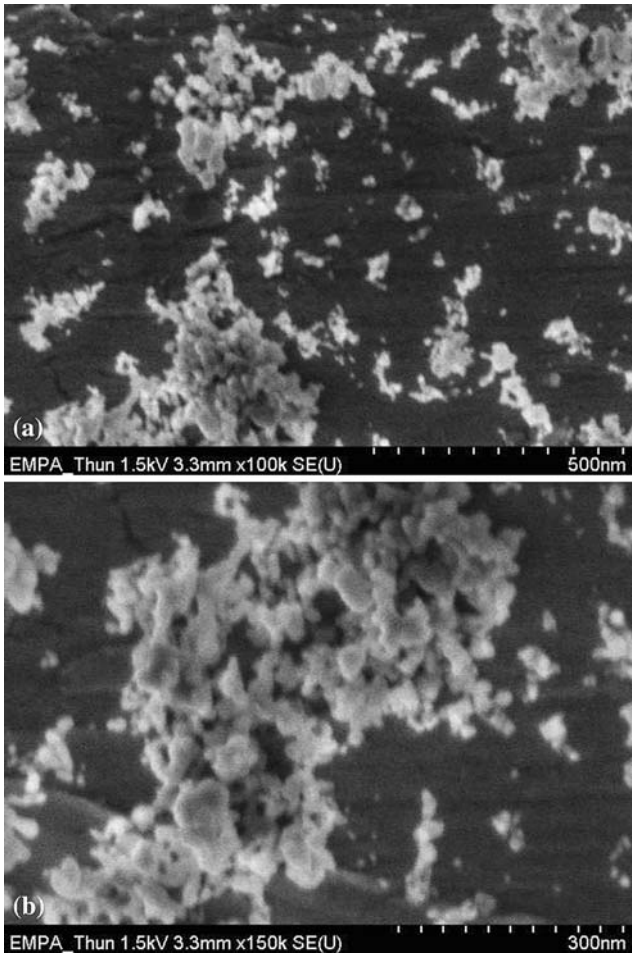

Fig. 10 Morphology of dried alumina suspension. (a) 10 wt.%. (b) 40 wt.%

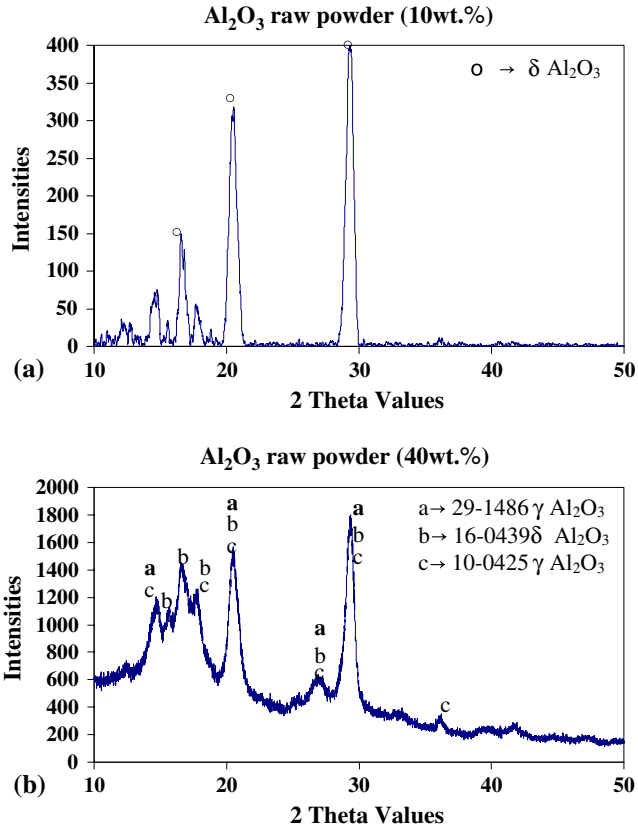

Fig. 11 XRD pattern of dried alumina suspension raw powder. (a) 10 wt.%. (b) 40 wt.%

agglomerated state and there were a lot of microcracks with submicron scales. This implies that the unmelted area in the coating caused the mechanical properties of the coating to degrade. The optical microscopic view of the cross-section interface of the coating is shown in Fig. 15, and x-ray diffraction (XRD) patterns of the surface is shown in Fig. 16. The peak of the alumina was broadening, and the main peak is from a stainless steel substrate. This means the microstructure of the surface had a nanoscale microstructure. The conditions of the experiment are listed in Table 3 (x-ray diffraction patterns).

The comparison between the two solvents can be made for a given plasma working condition. When water is used as a solvent, only unmelted particles could be seen (Fig. 12). That could be expected as water characteristics differ from those of ethanol, especially boiling temperature, surface tension, specific heat, and enthalpy of vaporization, which are higher in the case of water (Ref 32, Fig. 13). The fine crystal (Fig. 13c) size distribution characteristic is illustrated in Fig. 17.

Finally, the experiment on the influence of other parameters on the microstructure of the coating was carried out. The results were:

1. When the diameter of the needle was bigger than 0.4 mm, the injection had a great effect on the direction and the temperature of the plasma, and the melted droplets could not be collected. When the diameter of the needle was less than 0.14 mm, the needle was very easily blocked because the nanoparticles were adsorbed of the inner surface of the needle.
2. When the power of plasma was lower than 40 kW, a lot of unmelted splats could be collected at different distances (30-90 mm) when both water and ethanol were used as solvents (Fig. 18).
3. All particles collected at the distance between 20 and 40 mm (Fig. 18) were unmelted. A lot of droplets collected at the distances between 80 and 100 mm appeared to be spherical without impacting deformation, or only a little flattened.

4. Conclusions

1. Suspensions of nanoscale particles have very different flowing properties compared to the pure solvent. Because of the high surface-to-volume ratio, the nanoparticles are very easily absorbed at the inner surface of the needle, which can make the needle

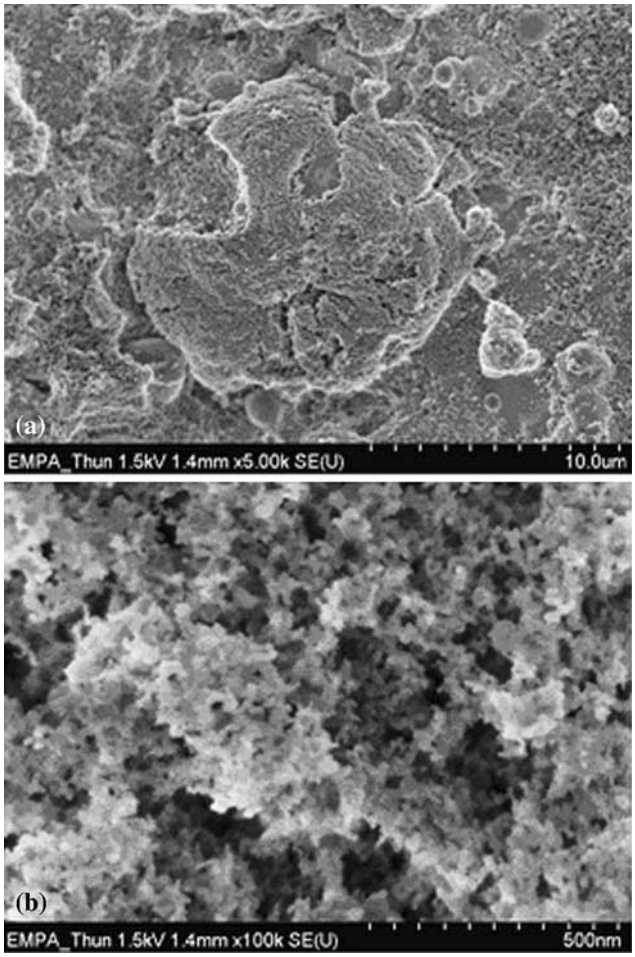

Fig. 12 Photographs of alumina water suspension coating surface at low magnification (a) and high magnification (b)

Table 2 Operating conditions—water used as solvent

Plasma power, kW	45
Plasma current, A	600
Ar, slpm	40
H_2, slpm	8
Distance, mm	60
Concentration, wt.%	10
Nozzle diameter, mm	6

(inner diameter 0.2 mm) close after about 20 min of operation.

2. The resistance of the boundary layer of the plasma near the substrate has a significant effect on the impact velocity of nanoscale droplets, which can immediately decelerate the velocity as soon as they are near the substrate. For alumina, the resistance can immediately decelerate the velocity of nanoparticles ($d < 60$ nm) to zero. In similar conditions, the impacting velocity of nanoparticles is lower when compared with their conventional powders. This implies that the interface formed by nanoscale droplets is weaker compared with their conventional coatings. Subsequently, this kind of coating shows lower macromechanical properties when compared with their conventional spraying coatings.
3. The concentration of alumina suspension is a key parameter for plasma suspension coatings. The low concentration causes the droplet size distribution to decrease, a low sum of enthalpy for vaporizing and melting in plasma spraying processes, and a smooth coating surface. This is beneficial for fine nanostructured coatings. However, on the other hand, low concentration means low spraying efficiency. In the experimental conditions, the optimized concentration of alumina suspension for plasma spraying was between 5 and 10 wt.%.
4. Besides the substrate temperature, the plasma spraying distances had an influence on the transformation of alumina phases in suspension spraying processes. In the experimental conditions (plasma power less than 50 kW), it was difficult to manufacture hardness α-alumina nanostructured coatings by changing the suspension spraying distance and plasma power. Transition γ-alumina, η-alumina, and θ-alumina are the main phases in alumina suspension plasma spray coatings and depend on the spraying distance.
5. With the use of peristaltic pump injection system and atmospheric plasma spraying, the fine nanostructured alumina ceramic coating, with the scale between 30 and 100 nm, would be fabricated in some areas. The solvent had a great influence on the microstructure of alumina suspension plasma spray coatings. When water was used as a solvent, the droplets were unmelted until the plasma power reached 45 kW. Ethanol was better for suspension plasma spraying coatings. Furthermore, the spraying distance and the plasma power seemed to have a significant effect on the coatings microstructure. The bigger plasma power (more than 45 kW) and 60-80 mm of spraying distance was better for the microstructure of alumina suspension plasma spray coatings.
6. In the injection system derived by a peristaltic pump, the pump rotation was a key parameter. The pressure fluctuation caused by rotation was not over 0.3 bar, which had little effect on the velocity of the injection. When the rotation reached 100 rpm (the inner diameter of tube was 3.2 mm, the inner diameter of the needle was 0.29 mm), the velocity of the injection was so high that it changed the direction of the plasma.
7. The quality of the coatings strongly depended on the plasma power, spraying distance, solvent, concentration, inner diameter of the needle, and pump rotation. The optimized working conditions are: on plasma power above 45 kW, the spraying distance between 60 and 80 mm, the inner diameter of needle between 0.2 and 0.29 mm, the pump rotation between 50 and 70 rpm, and the concentration between 5 and 10 wt.% and ethanol used as the solvent.

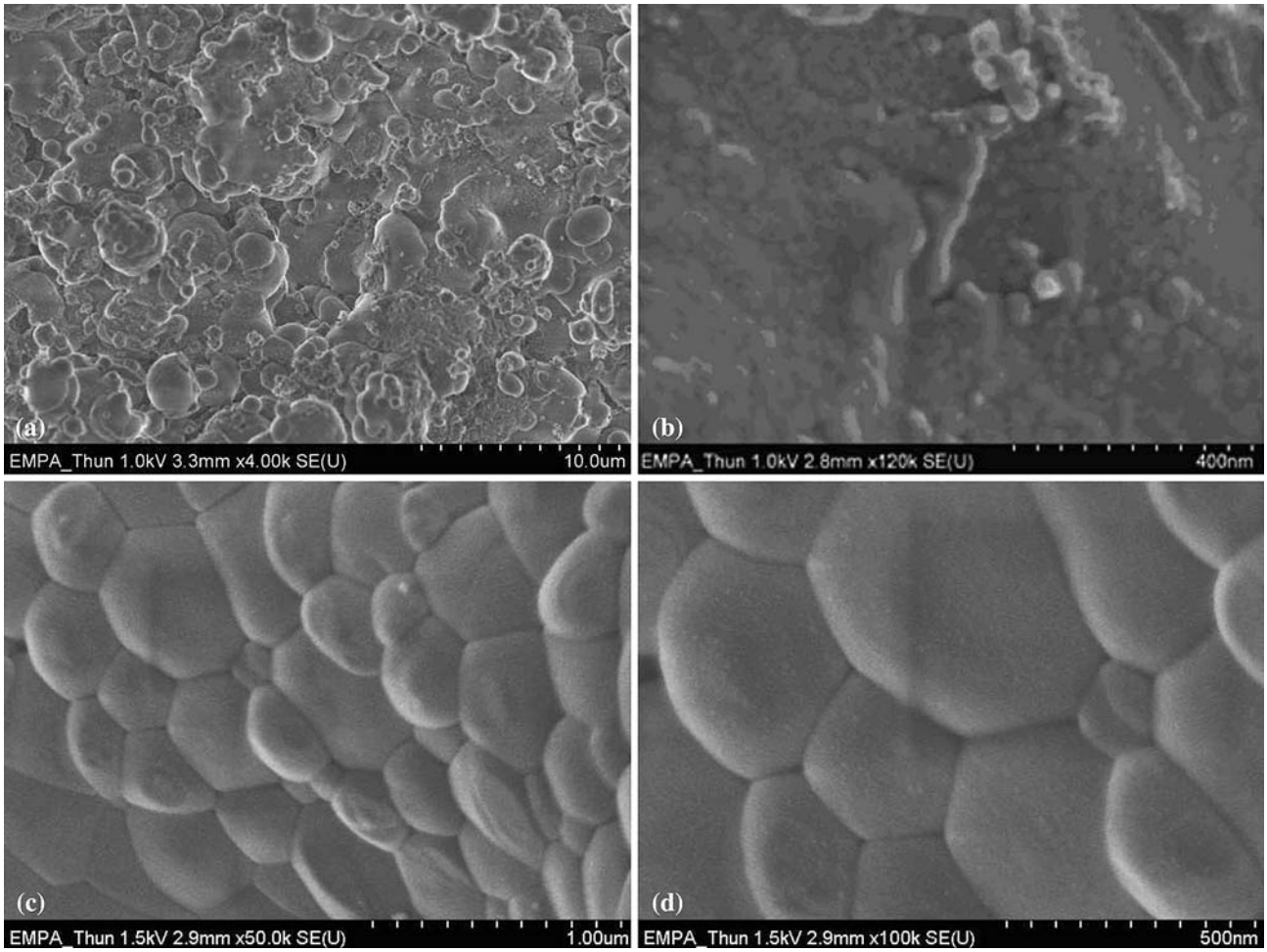

Fig. 13 Photographs of alumina ethanol suspension plasma spray coating surfaces at low magnification (a) and high magnification (b), (c), and (d)

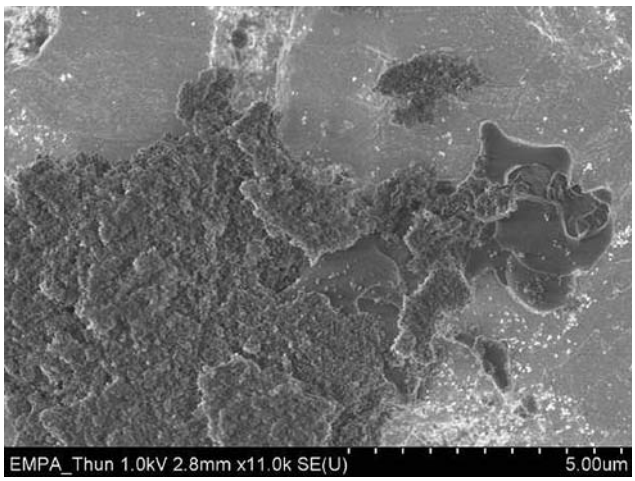

Fig. 14 Melted and unmelted areas of alumina ethanol suspension plasma spray coatings

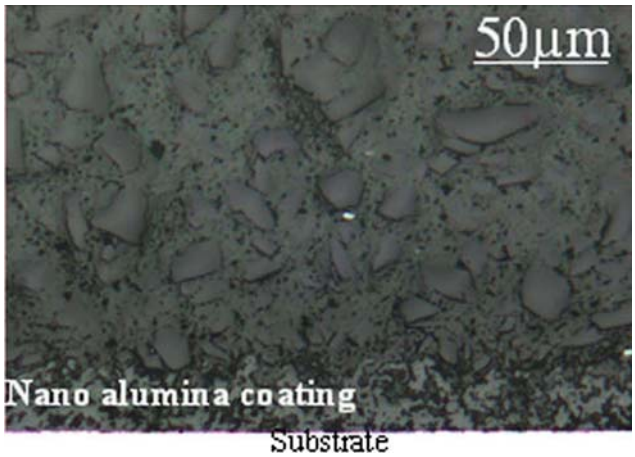

Fig. 15 Optical microscopy cross section of the interface of alumina ethanol suspension plasma spraying coating

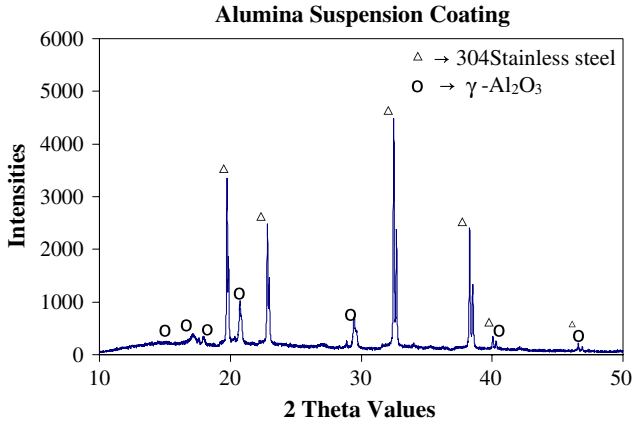

Fig. 16 XRD pattern of alumina ethanol suspension coatings

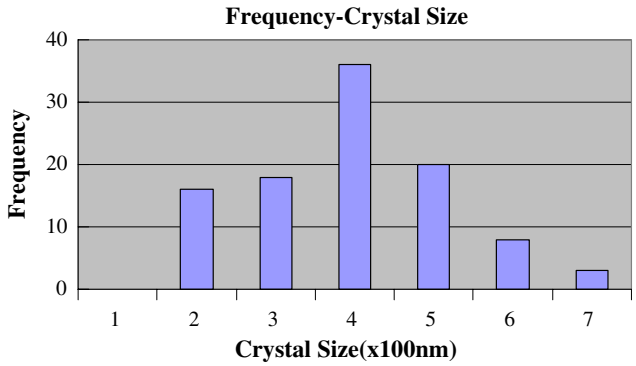

Fig. 17 Crystal size distribution of coating

Table 3 Operating conditions—sprayed with ethanol suspension

Plasma power, kW	48
Plasma current, A	700
Ar, slpm	40
H_2, slpm	8
Distance, mm	60
Concentration, wt.%	10
Nozzle diameter, mm	6

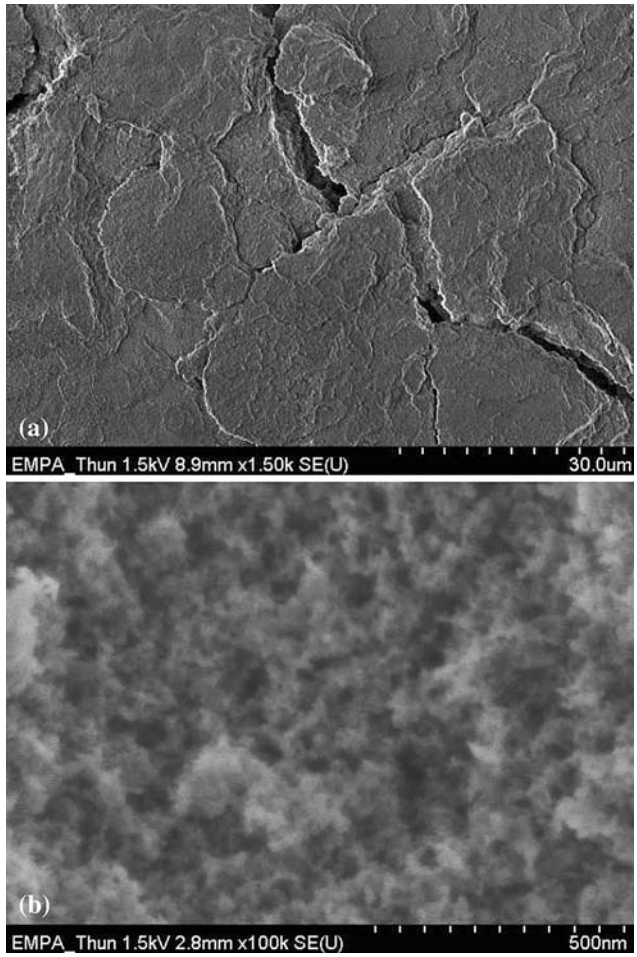

Fig. 18 Microstructure of alumina water suspension coating at low magnification (a) and high magnification (b). 17 kW, distance 40 mm, Ar/H_2 40/10 slm

Acknowledgments

The technical assistance (doing SEM images, plasma spraying system) of Dr. Christian Jaeggi and M. Bernhard Von Gunten from EMPA Thun Switzerland is gratefully acknowledged.

References

1. Y. Gao, X. Xu, Z. Yan, and G. Xin, High Hardness Alumina Coatings. Prepared by Low Power Plasma Spraying, *Surf. Coat. Technol.*, 2002, **2002**(154), p 189-193
2. K. Wittmann, F. Blein, J.F. Coudert, and P. Fauchais, Control of the Injection of an Alumina Suspension Containing Nanograins in a dc Plasma. *Thermal Spray 2001: New Surface for a New Millennium*, C.C. Berndt, K.A. Khor, and E.F. Lugscheider, Eds., ASM International, Materials Park, OH, 2001, p 375-382
3. C.-J. Li, G.-J. Yang, and Z. Wang, Effect of Spray Parameters on Structure of Nanostructured TiO_2 Deposits by Liquid Plasma Spray Process, *International Thermal Spray Conference Proceedings*, E. Lugscheider, Ed. (Essen, Germany), DVS-Verlag, 2002, p 544-549
4. M. Roy, A. Pauschitz, J. Bernardi, T. Koch, and F. Franek, Microstructure and Mechanical Properties of HVOF Sprayed Nanocrystalline Cr_3C_2-25 Coating, *J. Therm. Spray Technol.*, 2006, **15**(3), p 372-381
5. R.S. Lima and B.R. Marple, Superior Performance of High-Velocity Oxyfuel-Sprayed Nanostructured TiO_2 in Comparison to Air Plasma-Sprayed Conventional Al_2O_3-13TiO_2, *J. Therm. Spray Technol.*, 2005, **14**(3), p 397-403
6. C. Suryanarayana, The Structure and Properties of Nanocrystalline Materials: Issues and Concerns, *JOM*, 2002, **54**(9), p 24-27
7. D. Levchuk, Plasma Assisted Techniques for Deposition of Superhard Nanocomposite Coating, *Surf. Coat. Technol.*, 2007, **201**, p 6071-6077
8. P.H. Mayrhofer, C. Mitterer, and H. Clemens, Self-Organized Nanostructures in Hard Ceramic Coatings, *Adv. Eng. Mater.*, 2005, **7**(12), p 1071-1082
9. E.H. Jordan, M. Gell, Y.H. Sohn, D. Goberman, L. Shaw, S. Jiang, M. Wang, T.D. Xiao, Y. Wang, and P. Strutt, Fabrication

and Evaluation of Plasma Sprayed Nanostructured Alumina-Titania Coating with Superior Properties, *Mater. Sci. Eng. A*, 2001, **301**, p 80-89
10. T.C. Zhu, K. Yukimura, C.X. Ding, and P.Y. Zhang, Tribological Properties of Nanostructured and Conventional WC-Co Coating Deposited by Plasma Spraying, *Thin Solid Films*, 2001, **388**, p 277-282
11. H. Chen and C.X. Ding, Nanostructured Zirconia Coatings Prepared by Atmospheric Plasma Spraying, *Surf. Coat. Technol.*, 2002, **150**, p 31-36
12. M. Roy, A. Pauschitz, J. Wernisch, and F. Franek, The Influence of Temperature on the Wear of Cr_3C_2-25 (NiCr) Coating—Comparison Between Nanocrystalline Grains with Conventional Grains, *Wear*, 2004, **257**, p 799-811
13. G. Ji, O. Elkedim, and T. Grosdidier, Deposition and Corrosion Resistance of HVOF Sprayed Nanocrystalline Iron Aluminide Coatings, *Surf. Coat. Technol.*, 2005, **190**(2-3), p 406-416
14. Z.-G. Ban and L.L. Shaw, Characterization of Thermal Sprayed Nanostructured WC-Co Coatings Derived from Nanocrystalline WC-18wt.% Co Powders, *J. Therm. Spray Technol.*, 2003, **12**(1), p 112-119
15. S.-Q. Fan, G.-J. Yang, C.-J. Li, G.-J. Liu, C.-X. Li, and L.-Z. Zhang, Characterization of Microstructure of Nano-TiO_2 Coating Deposited by Vacuum Cold Spraying, *J. Therm. Spray Technol.*, 2006, **15**(4), p 513-517
16. S. Tao, B. Liang, C.X. Ding, H. Liao, and C. Coddet, Wear Characteristics of Plasma-Sprayed Nanostructured Yttria Partially Stabilized Zirconia Coatings, *J. Therm. Spray Technol.*, 2005, **14**(4), p 518-523
17. M. Gell, E.H. Jordan, Y.H. Sohn, and D. Goerman, Development and Implementation of Plasma Sprayed Nanostructured Ceramic Coatings, *Surf. Coat. Technol.*, 2001, **146-147**, p 48-54
18. R. Soltani, E. Garcia, T.W. Coyle, J. Mostaghimi, R.S. Lima, B.R. Marple, and C. Moreau, Thermomechanical Behavior of Nanostructured Plasma Sprayed Zirconia Coating, *J. Therm. Spray Technol.*, 2006, **15**(4), p 657-662
19. F.L. Toma, G. Bertrand, D. Klein, C. Coddet, and C. Meunier, Nanostructured Photocatalytic Titania Coating Formed by Suspension Plasma Spraying, *J. Therm. Spray Technol.*, 2006, **15**(4), p 587-591
20. R. Rampon, F.L. Toma, G. Bertrand, and C. Coddet, Liquid Plasma Sprayed Coatings of Yttria-Stabilized Zirconia for SOFC Electrolytes, *J. Therm. Technol.*, 2006, **15**(4), p 682-688
21. J. Oberste Berghaus, B. Marple, and C. Moreau, Suspension Plasma Spraying of Nanostructured WC-12Co Coatings, *J. Therm. Spray Technol.*, 2006, **15**(4), p 6676-6682
22. P. Fauchais, Suspension and Solution Plasma or HVOF Spraying, *J. Therm. Spray Technol.*, 2008, **17**(1), p 1-3
23. V. Rat, C. Delbos, J. Fazilleau, J.F. Coudert, and P. Fauchais, Dense Zirconia Electrolyte by Suspension D.C. Plasma Spraying, *XII. Workshop Plasmatechnik*, Sept 23-24, 2004, p 89-103
24. V.V. Sobolev and J.M. Guilemany, Flattening of Droplets and Formation of Splats in Thermal Spraying: A Review of Recent Work—Part 1, *J. Therm. Spray Technol.*, 1999, **8**(1), p 87-100
25. J. Oberste Berghaus, S. Bouaricha, J.-G. Legoux, and C. Moreau, Suspension Plasma Spraying of Nanoceramics Using an Axial Injection Torch, *Thermal Spray Connects: Explore Its Surfacing Potential,* E. Lugscheider and C.C. Berndt, Eds., May 2-4, 2005 (Basel, Switzerland), ASM International, Materials Park, OH, 2005
26. B. Samareh and A. Dolatabadi, A Three-Dimensional Analysis of the Cold Spray Process: Effect of Substrate Location and Shape. *Thermal Spray 2007: Global Coating Solutions*, B.R. Marple, M.M. Hyland, Y.-C. Lau, C.-J. Li, R.S. Lima, and G. Montavon, Eds., ASM International, Materials Park, OH, 2007, p 634-642
27. X. Jang, *Fluid Dynamics*, Mechanical Industrial Press, China, 1986, p 245-267
28. K.E. Schneider, V. Belashchenko, M. Dratwinski, S. Siegmann, and A. Zagorski, *Thermal Spraying for Power Generation Components*, Wiley-VCH Verlag GmbH & Co. KGaA, Weinheim, 2006, p 289-301
29. C.-J. Li, A. Ohmori, and Y. Harada, Experimental Investigation of the Morphology of Plasma Sprayed Copper Splat, *Proc. 14th International Thermal Spray Conference*, A. Ohmori, Ed. (Kobe, Japan), Japan High Temperature Society, 1995, p 333-339
30. C.-J. Li, H.-L. Liao, P. Gougeon, G. Montavon, and C. Coddet, Effect of Reynolds Number of Molten Spray Particles on Splat Formation in Plasma Spraying. *Thermal Spray 2003: Advancing the Science Applying the Technology*, C. Moreau and B. Marple, Eds., ASM International, Materials Park, OH, 2003, p 875-882
31. C. Delbos, J. Fazilleau, J.F. Coudert, P. Fauchais, L. Bianchi, and K. Wittmann, Plasma Spray Elaboration of Finely Structured YSZ Thin Coating by Liquid Suspension Injection. *Thermal Spray 2003: Advancing the Science and Applying the Technology*, C. Moreau and B. Marple, Eds., ASM International, Materials Park, OH, 2003, p 661-669
32. K. Wittman, F. Blein, J. Fazilleau, J.-F. Coudert, and P. Fauchais, A New Process to Deposit Thin Coatings by Injecting Nanoparticles Suspensions in a DC Plasma Jet, *Proc. International Thermal Spray Conference (ITSC '02)*, E. Lugscheider, Ed. (Essen, Germany), DVS Düsseldorf, 2002, p 519-522
33. C.-J. Li, Y.-Y. Wang, T. Wu, and A. Ohmori, Effects of Surface Melting Particles on Adhesion of Ceramic Coating by High Velocity Oxy-Fuel Spraying, *J. Xi'an Jiaotong University*, 2001, **1**, p 51-55
34. Y. Shan, T.W. Coyle, and J. Mostaghimi, Numerical Simulation of Droplet Break up and Collision in the Solution Precursor Plasma Spraying Process. *Thermal Spray 2007: Global Coating Solutions*, B.R. Marple, M.M. Hyland, Y.-J. Li, R.S. Lima, and G. Montavon, Eds., ASM International, Materials Park, OH, 2007, p 698-704
35. C. Robert, A. Denoirjean, A. Vardelle, G.X. Wang, and S. Sampath, Nucleation and Phase Selection in Plasma-Sprayed Alumina: Modeling and Experiment, *15th International Thermal Spray Conference*, C. Coddet, Ed., May 24-29, 1998 (Nice, France), IPSE, ASM International, Materials Park, OH, 1998, p 407-412